JACS
JOURNAL OF THE AMERICAN CHEMICAL SOCIETY

Article

pubs.acs.org/JACS

Intracellular Protein-Responsive Supramolecules: Protein Sensing and In-Cell Construction of Inhibitor Assay System

Tatsuyuki Yoshii,[†] Keigo Mizusawa,[†] Yousuke Takaoka,*[,‡] and Itaru Hamachi*[,†,§]

[†]Department of Synthetic Chemistry and Biological Chemistry, Kyoto University, Katsura, Nishikyo-Ku, Kyoto 615-8510, Japan
[‡]Department of Chemistry, Tohoku University, 6-3 Aramaki-aza Aoba, Aoba-ku, Sendai 980-8578, Japan
[§]Japan Science and Technology Agency (JST), CREST, 5 Sanbancho, Chiyoda-ku, Tokyo 102-0075, Japan

Supporting Information

ABSTRACT: Supramolecular nanomaterials responsive to specific intracellular proteins should be greatly promising for protein sensing and imaging, controlled drug release or dynamic regulation of cellular processes. However, valid design strategies to create useful probes are poorly developed, particularly for proteins inside living cells as targets. We recently reported a unique supramolecular strategy for specific protein detection using self-assembling fluorescent probes consisting of a protein ligand and a fluorophore on the live cell surface, as well as in test tube settings. Herein, we discovered that our self-assembled supramolecular probes having a rhodamine derivative (tetramethylrhodamine or rhodamine-green) can incorporate and stay as less-fluorescent aggregates inside the living cells, so as to sense the protein activity in a reversible manner. Using the overexpressed model protein (dihydrofolate reductase), we demonstrated that this turn-on/off mode is controlled by selective ligand−protein recognition inside the live cells. Not only such a model protein, but also endogenous human carbonic anhydrase and heat shock protein 90 were specifically visualized in living mammalian cells, by use of the similar ligand-tethered supramolecular probes. Furthermore, such reversibility allowed us to intracellularly construct a unique system to evaluate the inhibitors affinity toward specific endogenous proteins in live cells, highlighting the potential of dynamic supramolecules as novel intelligent biomaterials.

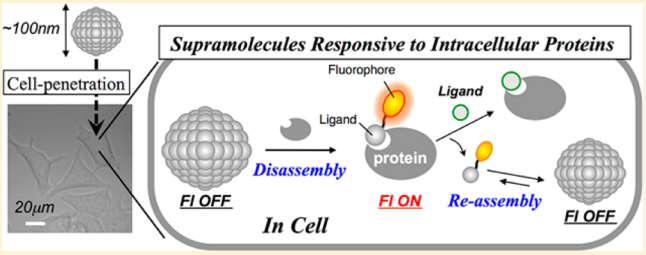

INTRODUCTION

Proteins are involved in all biological events, and as such, their localization, expression level and functions are dynamically regulated in live cells.[1,2] Therefore, protein-responsive materials should hold promise for specific protein sensing, live imaging, controlled drug release, and regulation of cellular processes.[3,4] The use of supramolecular nanomaterials in response to selective proteins in live cells is attractive because of their dynamic reversibility and potentially high biodegradability.[5,6] Cell surface proteins as therapeutic and/or diagnostic biomarkers are easiliy accessible for synthetic biomaterials, and thus, many promising nanomaterials have been developed.[7,8] In contrast, intracellular proteins are known to be extremely difficult to target, and the development of supramolecular nanomaterials that are responsive to "intracellular proteins" remains challenging. There are various obstacles that must be overcome for nanomaterials to be workable inside living cells, including sufficient cell permeability through biomembranes, high target protein specificity under crude intracellular conditions, and effective switching functions that are operatable inside live cells. As pioneering works, enzymatic reaction-triggered self-assembling nanostructures that function inside living cells have been reported by Rao et al., in which an intracellular protease initiates the deprotection reaction of precursor molecules to yield covalently linked fluorescent oligomers.[9,10] Xu et al. have succeeded in the formation of phosphatase-triggered supramolecular hydrogels in live cells, demonstrating their use in an activity assay for the cytosolic enzyme.[11,12] Aggregation-induced emission resulting in a turn-on fluorescence in response to a target enzyme was also recently applied to specific protein sensing in live cells.[13−15] Although these examples indicate the successful formation of supramolecular nanostructures in living cells, reversible self-assembly/disassembly of such materials has never been achieved. Reversible self-assembly/disassembly would be a desirable feature of supramolecular nanomaterials, and could lead to various applications including dynamic protein sensing in response to the expression level, protein activity or protein-triggered intracellular drug release.

We recently developed a disassembly driven turn-on nanoprobe, where the ligand-tethered fluorophores exhibited unique self-assembling features and showed a reversible turn-on fluorescent change toward nonenzymatic-proteins on a live cell surface, as well as toward purified ones in a test tube.[16−19] However, we have not yet succeeded in demonstrating that our nanoprobes can penetrate the cell membrane efficiently, and bind selectively and reversibly to the target protein inside the

Received: September 7, 2014
Published: October 31, 2014

   dx.doi.org/10.1021/ja508955y | J. Am. Chem. Soc. 2014, 136, 16635−16642

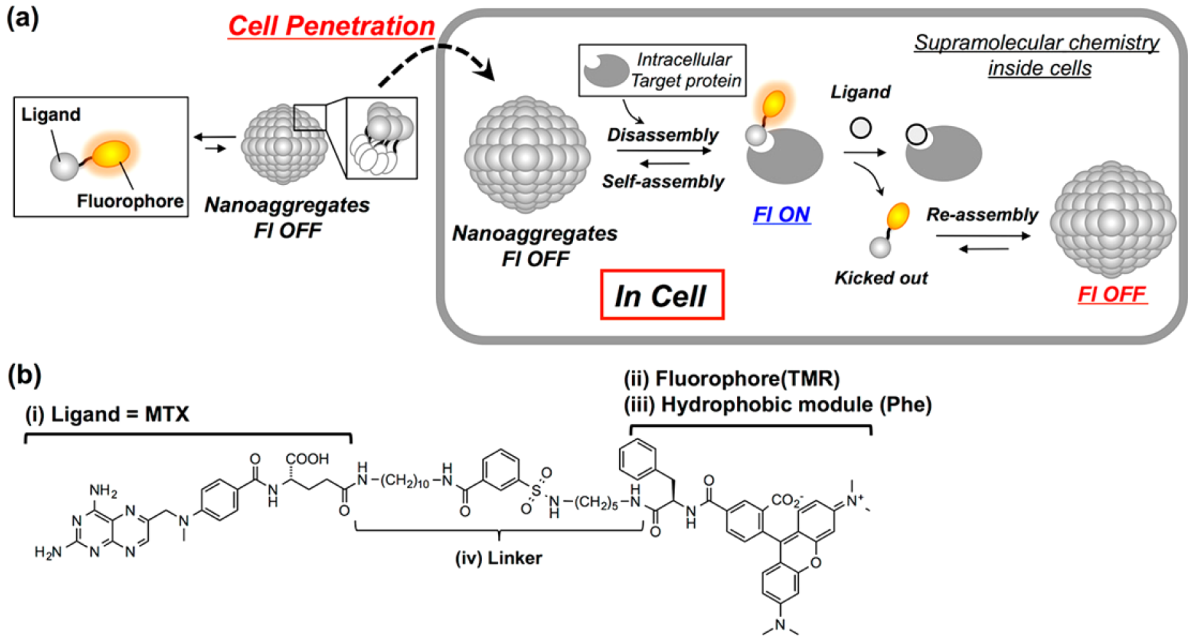

Figure 1. Protein-responsive nanoaggregates for specific and reversible intracellular protein sensing. (a) Schematic illustration of in cell reversible protein sensing by self-assembling nanoaggregates. (b) Chemical structure of ligand-tethered probe **1** for intracellular eDHFR imaging.

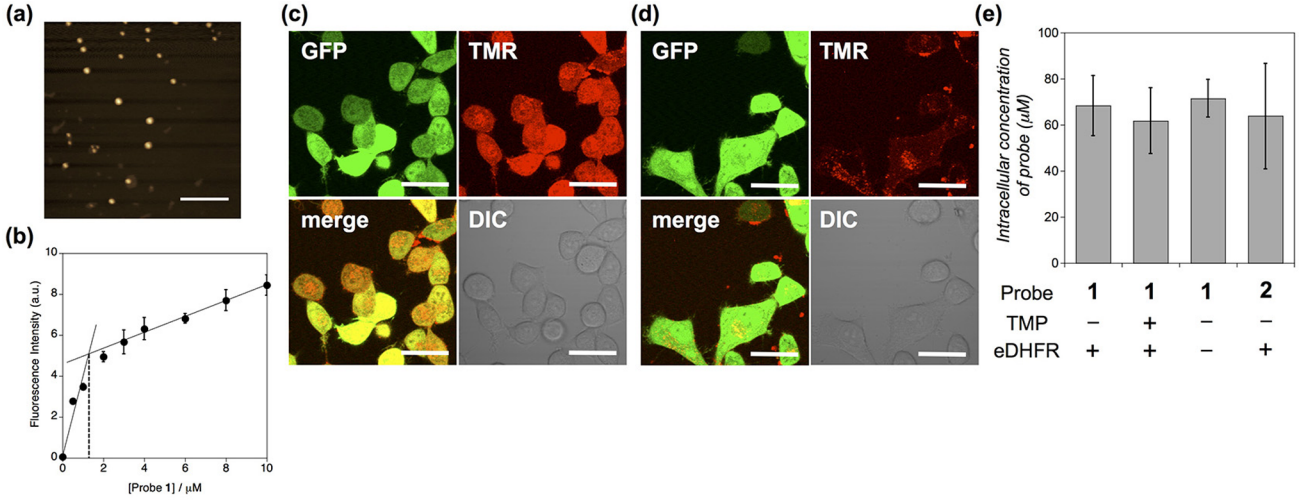

Figure 2. Fluorescent imaging of intracellular eDHFR-GFP using probe **1** in living cells. (a) Atomic force microscopy (AFM) image of the self-assembled probe **1** (10 μM) (scale bar 500 nm). (b) Concentration-dependent fluorescent intensity change of 1 (0−10 μM, λ_{em} = 584 nm). (c) CLSM images of HeLa-DG cells treated with probe **1** (2 μM) for 12 h at 37 °C. The images were obtained without any washing (scale bars, 20 μm). (d) CLSM images of HeLa-DG cells treated with probe 1 (2 μM) for 12 h at 37 °C, and then treated with TMP (10 μM). The images were obtained without any washing (scale bars, 20 μm). (e) Intracellular concentration of incorporated probe **1** or **2** in HeLa-DG cells or normal HeLa cells, calculated with fluorescent spectra of these cell lysates. The experiments were performed in triplicate to obtain mean and standard deviation values (shown as error bars).

cells. On the basis of elaborate molecular design and careful physicochemical analyses, we herein reveal that the self-assembling nanoaggregates can operate well inside living cells; that is, "intracellular" proteins detection and imaging were carried out with turn-on manner. From the model experiments using overexpressed dihydrofolate reductase (eDHFR), it was clear that (1) the probe can be incorporated into the inside cells by an endocytosis mechanism, and (2) self-assembly/disassembly of the nanoaggregates indeed occurred reversibly in living cells upon a specific ligand−protein recognition (Figure 1a). More importantly, we also succeeded in specific imaging of endogenously expressed intracellular proteins such as human carbonic anhydrase (hCAII) and heat shock protein 90 (HSP90). An imaging-based inhibitor assay for these endogenous proteins using live cells was constructed, clearly highlighting the advantage of incorporating a reversible assembly/disassembly function in the design of sophisticated supramolecular biomaterials.

RESULTS AND DISCUSSION

Self-Assembling Rhodamine-Based Supramolecule Is Capable of Turn-on Sensing of eDHFR Inside the Living Cells. We previously reported that our ligand-tethered probes bearing self-assembling property allowed for rapid and

dx.doi.org/10.1021/ja508955y | J. Am. Chem. Soc. 2014, 136, 16635−16642

convenient turn-on fluorescent imaging of membrane-bound endogenous protein on the live cell surface for a short-time observation. In case of probe **1** having methotrexate (MTX) as a ligand for membrane-bound folate receptor, for example, strong fluorescence could be detected only from the KB cell surface (endogenously expressing folate receptor) within 1 h. On the other hand, we noticed that fluorescent granules were also weakly observed inside of the cells for the longer incubation time (about 12 h) for both KB cell and other cell line not-expressing folate receptor. This indicated that the probes can be internalized into live cells with retaining the suppressed fluorescence, which suggested us an interesting possibility that some of our self-assembling probes may be applicable even to "intracellular protein" sensing. We thus initially examined the self-assembly/disassembly behavior of the fluorescent probe **1** inside of the living cells. In detail, this probe **1** is composed of the following four modules: (i) methotrexate (MTX) as a hydrophilic ligand for targeting not only folate receptor, but also eDHFR used here as an intracellular model protein, (ii) tetramethylrhodamine (TMR) as a zwitterionic fluorophore for imaging, (iii) phenylalanine as a hydrophobic module for finely tuning the aggregation property, and (iv) a relatively hydrophobic linker for connecting these modules (Figure 1b).[19] We confirmed that probe **1** formed spherical or oval aggregates with a mean diameter of 40 nm, and had a critical aggregation concentration (CAC) lower than 1.31 μM (Figure 2a,b and Figure S1a,b, Supporting Information). The fluorescence of probe **1** was greatly suppressed owing to self-aggregation and was enhanced by 37-fold upon addition of purified eDHFR in a test tube (Figure S1c−e).[19] The detection limit of **1** for eDHFR was 66 nM (Figure S1f).

A HeLa cell line stably overexpressing GFP-fused eDHFR (HeLa-DG cell) was employed in this model study.[20] From the confocal laser scanning microscopy (CLSM) image using the GFP channel, it was evident that eDHFR-GFP was distributed throughout the entire cell including the cytosol and nuclei.[20] When probe **1** was added to HeLa-DG cells and incubated for 12 h at 37 °C, strong TMR fluorescence was observed by CLSM from the intracellular regions without any washing, which completely merged with the image obtained from the GFP emission (Figure 2c). Under these conditions, serious cytotoxicity was not observed (Figure S1g). The fluorescence intensity inside the cells dramatically decreased upon addition of trimethoprim (TMP), a strong inhibitor for eDHFR,[21,22] without any intensity changes in the fluorescence of the extracellular region (Figure 2d). In a negative control using normal HeLa cells lacking eDHFR-GFP, only fluorescent granules were weakly observed (Figure S2a). On the basis of these results, it was concluded that **1** is capable of fluorescently imaging eDHFR inside the HeLa cells in the turn-on mode through MTX-eDHFR specific interactions. Quantitative evaluation of the amount of **1** transported into the live cells revealed that almost the same amount of probe **1** entered these cells regardless of the presence or absence of the target eDHFR, and the incorporated probe **1** remained in the HeLa cell interior and was not released, even in the presence of the inhibitor (TMP) (Figure 2e). We also determined the concentration of **1** per single cell to be over 60 μM, which was higher than the CAC of **1** (<1.31 μM, Figure 2b and e). Given all of the results here obtained, we considered that (1) the probe **1** was transported into the cells independent of eDHFR and self-assembled in the absence of eDHFR inside cells, (2) disassembly of the nanoaggregates was driven by ligand-eDHFR recognition in the presence of eDHFR, triggering the turn-on fluorescence change, and (3) **1** was released out of the eDHFR binding pocket by exchange with the competitive inhibitor, which resulted in the reassembly of **1** inside the living cells. Consequently, the fluorescence was turned off although the weak granulated fluorescence was still present as background noise (Figure 1a).

In order to further evaluate any impacts of self-assembling property of the probe **1** on the cell-penetration efficiency and retention ability inside the cells, we employed an always-on (nonassembling) probe **1′** (Figure S3) and a self-assembled but nonrecognizable probe **2** (under-mentioned). In case of the always-on-type probe **1′**, intracellular eDHFR cannot be clearly visualized mainly due to its high background signal from the extracellular region (Figure S3e). Also, the amount of incorporated probe **1′** per single HeLa-DG cell was too small to be determined by the method applied for the probe **1**, which was lower than 2 μM.[23] On the other hand, in the case of probe **2** that is a nonrecognition self-assembling probe tethering not eDHFR ligand but hCA ligand, almost the same amount of probe was incorporated in HeLa-DG cell (64 μM, Figure 2e) as the case of probe **1**, regardless of no ligand/protein recognition. Given these results, it was clear that (i) the self-assembly property may contribute to both the enhanced cell-penetration and the probe retention inside the cells, and (ii) the protein binding does not strongly impact on the probe retention in cells. These should give important clues for designing supramolecular self-assembly workable in live cell systems.

Mechanisms of Internalization and Turn-on Sensing of Probe 1 with eDHFR in Cells. To explore the transport mechanism of the self-assembling probe **1** into the HeLa-DG cells, time-lapse fluorescent live imaging was performed. As shown in Figure 3a, upon addition of probe **1** (after a few minutes), weak fluorescence was only observed from the cell membrane, and after 20 min at 37 °C, several fluorescent granules subsequently appeared inside the cells. The punctum fluorescence gradually became more homogeneous and was distributed in the whole cytosol. The cytosolic fluorescence gradually increased in intensity until 12 h, while the membrane fluorescence relatively lessened and was indistinguishable from the cytosolic one (Figure 3b). In the case of cells treated with **1** at 4 °C, the intracellular fluorescence was negligible even after a 5 h incubation, whereas weak fluorescence was observed on the cell membrane (Figure S2b). On the other hand, weak but distinct fluorescent granules were observed from normal HeLa cells (lacking eDHFR-GFP) as shown above merged with that of Lysotracker green (Figure S2c). These results strongly suggested that endocytosis is the main pathway for the intracellular transport of probe **1**. More detailed analysis was conducted using various endocytosis inhibitors. After treatment of genistein or 5-(*N*-ethyl-*N*-isopropyl)-amiloride (EIPA), inhibitors for caveolae-mediated endocytosis[24] or macropinocytosis, respectively,[25,26] the fluorescence intensities of the cells stained with **1** were suppressed by less than the half compared with the cells incubated in the absence of inhibitors (Figure S4). In contrast, a decrease in fluorescence was not observed upon incubation with amantadine, an inhibitor for clathrin-mediated endocytosis.[27] Taken together, it suggested that **1** (or self-assembling nanoaggregates of **1**) internalized through caveolae-mediated endocytosis or macropinocytosis, both of which had been recently characterized as primary pathways for internalization of macromolecules such as proteins

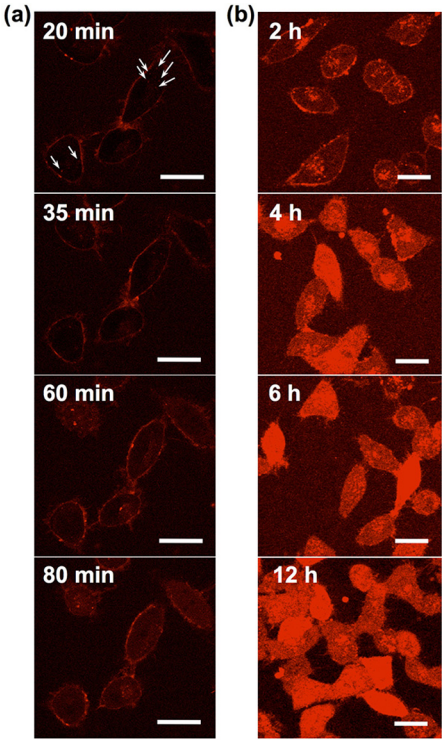

Figure 3. Time trace of eDHFR imaging in HeLa-DG cells stained by probe **1** incubated at 37 °C within (a) a short time period (20−80 min) and (b) a long time period (2−12 h). Scale bars, 20 μm.

or metal nanoparticles.[28,29] Thereafter, the internalized **1** would gradually escape from the endosomal vesicles to the cytosol. In the absence of the target eDHFR, most of **1** formed stable nonfluorescent aggregates whereas the aggregates disassembled into fluorescent **1**/eDHFR complexes in the presence of eDHFR, resulting in recognition-driven turn-on fluorescence inside the cells.

Intracellular Endogenous hCAII Sensing and In-Cell Inhibitor Assay by Self-Assembling Supramolceular Probe. The present success in imaging intracellular eDHFR as a model encouraged us to target more difficult proteins, that is, "endogenous" proteins inside of living cells. Cytosolic hCAII, a protein related to various diseases such as epilepsia or glaucoma was attempted. Using the same design strategy as the eDHFR probe, a TMR-tethered probe **2** carrying a benzenesulfonamide ligand, a selective inhibitor of the hCA family,[30] was prepared (Figure 4a). Atomic force microscopy (AFM) or dynamic light scattering (DLS) data revealed the formation of spherical or oval aggregates of **2** with a mean diameter of 100 nm in aqueous buffer (Figure 4b and S5a). The CAC value of **2** was determined to be lower than 110 nM (Figure S5b). We also confirmed that probe **2** showed a 30-fold increase in the fluorescent intensity in response to purified hCAII in a test tube (Figure 4c and S5c,d). The detection limit of **2** for hCAII was 67 nM (Figure S5e). Imaging of endogenous hCAII in live MCF7 cells, a human breast cancer cell line naturally expressing hCAII, was then conducted using probe **2**. When **2** was mixed with MCF7 cells followed by incubation for 4 h at 37 °C, strong fluorescence from TMR was observed in the cytosol region including the nucleus by CLSM (Figure 4d). The strong fluorescence inside the cells dramatically decreased upon addition of ethoxazolamide (EZA) (Figure 4e), an hCAII inhibitor,[30] implying that the

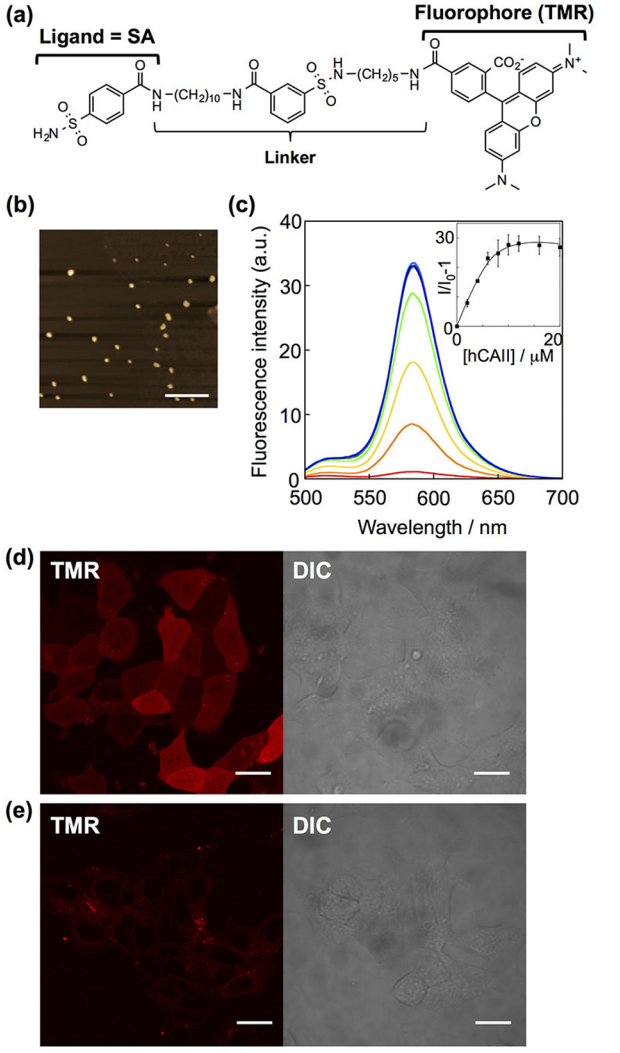

Figure 4. Endogenously expressed intracellular hCAII imaging by self-assembling nanoaggregates. (a) Chemical structure of ligand-tethered probe **2** for intracellular endogenous hCAII imaging. (b) AFM image of probe **2** (10 μM) in 50 mM HEPES buffer (pH 7.2, 150 mM NaCl). (c) Fluorescence spectra change of probe **2** (10 μM) upon addition of purified hCAII (0−20 μM) (λ_{ex} = 480 nm) in 50 mM HEPES buffer (pH 7.2, 150 mM NaCl). (Inset) The relative fluorescence intensity change was plotted with the concentration of hCAII. The experiments were performed in triplicate to obtain mean and standard deviation values (shown as error bars). (d) CLSM images of MCF7 cells treated with probe **2** (300 nM) for 4 h at 37 °C. The images were obtained without any washing (scale bars, 20 μm). (e) CLSM images of MCF7 cells treated with probe **2** (300 nM) for 4 h at 37 °C, and then treated with EZA (100 μM). The images were obtained without any washing (scale bars, 20 μm).

selective ligand-hCAII recognition was cruicial for the turn-on imaging, similar to the above-mentioned probe **1**.[31] These results demonstrated that an endogenously expressed intracellular protein can be visualized by our disassembly driven turn-on probe.[32]

Because of the reversible properties in living cells, a unique imaging-based inhibitor screening was next constructed using **2**. After staining with **2**, the MCF7 cells were incubated with an hCAII inhibitor such as EZA, acetazolamide (AAZ) or 4-sulfamoylbenzoic acid (SBA), followed by fluorescence monitoring by CLSM. When the strong inhibitor EZA was added, a significant decrease in the fluorescent intensity of the

dx.doi.org/10.1021/ja508955y | J. Am. Chem. Soc. 2014, 136, 16635−16642

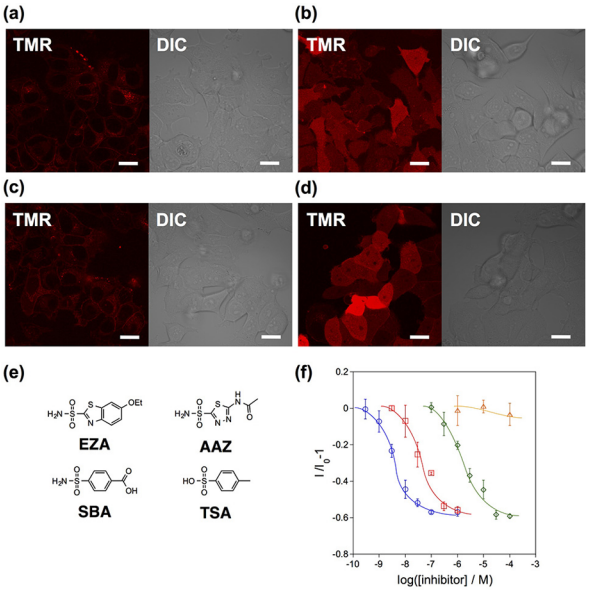

Figure 5. Imaging-based hCAII inhibitor assay with probe **2**. (a–d) Fluorescence images of MCF7 cells treated with probe **2** (100 nM), and then the cells were treated with hCAII inhibitors [(a) EZA (10 nM), (b) AAZ (10 nM), (c) AAZ (300 nM) and (d) SBA (1 μM)]. The images were obtained without any washing operations (scale bars, 20 μm). (e) Chemical structures of inhibitors for hCAII used in this study. EZA is 6-ethoxy-2-benzothiazolesulfonamide, AAZ is acetazolamide, SBA is 4-sulfamoylbenzoic acid, and TSA is 4-toluenesulfonic acid. (f) Fluorescence titration profile of the relative change in fluorescence intensity ($I/I_0 - 1$) from the intracellular region vs inhibitor concentration for EZA (○, blue), AAZ (□, red), SBA (◇, green) and noninhibitor TSA (△, orange). Fluorescence intensities were evaluated at 10 cells in 5 regions in each dish, and the experiments were performed in triplicate to obtain mean and standard error values (shown as error bars).

intracellular region was induced, which saturated in the nM concentration range as shown in Figure 5a and Figure S6. In contrast, no substantial change was observed by addition of 0.1 mM of *p*-toluenesulfonic acid (TSA), which has negligible affinity for the CA family (Figure 5f and Figure S9). We prepared the titration curve on the basis of the CLSM imaging changes, giving IC_{50} values (half maximal inhibitory concentration of fluorescence intensity change) of 9.9×10^{-9} M for EZA, 2.7×10^{-8} M for AAZ and 1.3×10^{-6} M for SBA, respectively (Figure 5b,c,d,f and S6–S8). The literature values (K_i) determined by using purified hCAII were reported to be 8×10^{-9} M (EZA), 1.2×10^{-8} M (AAZ) and 2.6×10^{-7} M (SBA).[30,33] While these K_i values for EZA or AAZ were almost the same as those obtained from our cell-based assay, the value for SBA was clearly different. This may be attributed to the fact that our method evaluated the lower cell-permeability and/or the lower in-cell selectivity of SBA, together with the simple affinity to CA, implying that the present cell-based inhibitor assays allow us to estimate the drug potencies under more real conditions. More importantly, these results strongly suggested that the reversible self-assembly/disassembly phenomenon of the supramolecular probes is powerful for sensing dynamic ligand/protein interactions, an essential function of endogenous proteins, even in the interior of living cells.

The flow cytometry analyses quantitatively supported our data from the cell imaging-based assay. The strong fluorescence was clearly observed from MCF7 cells stained with probe **2** and this fluorescence significantly decreased by addition of EZA (Figure S10a). The detailed titration curve was almost comparable to the CLSM analyses shown in Figure S10b. These results also implied that our reversible self-assembling probes can be used for the flow cytometer-based inhibitor screening systems for intracellular proteins, as well as the imaging-based assay.

Development of Nanoaggregates for Sensing of Endogenous HSP90 and In-Cell Construction of Anticancer Agent Screening System. Benefiting from the modular design, a self-assembling fluorescence turn-on probe was constructed by replacing the ligand part for another endogenously expressed intracellular protein, HSP90, a well-known tumor biomarker and valuable drug target for cancer diagnostics and treatment.[34,35] TMR-tethered probe **3** (λ_{em} = 585 nm) carrying PU-H71 as a ligand, a selective inhibitor of HSP90, was designed (Figure 6a).[36,37] It showed a 32-fold increase in fluorescent intensity by addition of the N-terminal ATP-binding domain of HSP90 (HSP90-N) (Figure 6b–d and Figure S11).[38,39] The CAC value of **3** was lower than 110 nM (Figure S11b). The detection limit of **3** for HSP90-N was 70 nM (Figure S11d). We then sought to fluorescently image endogenous HSP90 in live SK-BR-3 cells, a human breast cancer cell line,[40,41] using probe **3**. When probe **3** was mixed with SK-BR-3 cells, strong TMR fluorescence was detected in the cytosol area of SK-BR-3 cells by CLSM observation (Figure 6e). This image was almost identical to that of the immunostaining pattern obtained using an anti-HSP90 antibody (Figure S12a). The fluorescence intensity inside the cells was substantially decreased upon addition of PU-H71 (Figure 6f), suggesting that **3** was kicked out of the HSP90 binding pocket and reassembled into nanoaggregates, similar to probe **1** (for overexpressed eDHFR) and **2** (for endogenous hCAII).[42] Like the case of probe **2**, the flow cytometry analyses supported the results obtained by our cell image-based intensity analyses for the SK-BR-3 cells with probe **3** and PU-H71 (Figure S12c). Additionally, another turn-on probe **4**, which emitted a distinct color (λ_{em} = 530 nm) by replacing TMR with rhodamine-green (RhoG), can also be designed. This probe showed 350-fold fluorescent enhancement in response to HSP90-N (Figure S13) in test tube settings. By using probe **4**, an almost identical imaging pattern was obtained compared to probe **3** (Figure S14a).[43] These results clearly indicated that our self-assembling probe is capable of sensing endogenous intracellular proteins with varied colors (at least green and red colors), and these properties are good compatible with existing intracellular imaging technologies such as genetically encoded fluorescent protein tags.

The titration curves for several HSP90 inhibitors were obtained, allowing the determination of the IC50 values 2.1×10^{-6} M for PU-H71 and 8.1×10^{-6} M for MPC3100 (Figure 6h). In contrast, no substantial change was observed upon addition of 10 μM of geldanamycin, another inhibitor for HSP90. To date, various HSP90 inhibitors have been developed as anticancer agents, the potencies of which (typically as IC50 values) were examined by an indirect phenotype assay, such as via tumor cell growth inhibition (the reported values are 5×10^{-8} M for PU-H71,[36] 6×10^{-8} M for MPC-3100[44] and 2×10^{-9} M for geldanamycin,[45] respectively). To the best of our knowledge, the results described herein provide affinity values for HSP90 inhibitors toward active HSP90 in living cells for the first time. Ultimately, this methodology should prove helpful for direct drug discovery

dx.doi.org/10.1021/ja508955y | J. Am. Chem. Soc. 2014, 136, 16635–16642

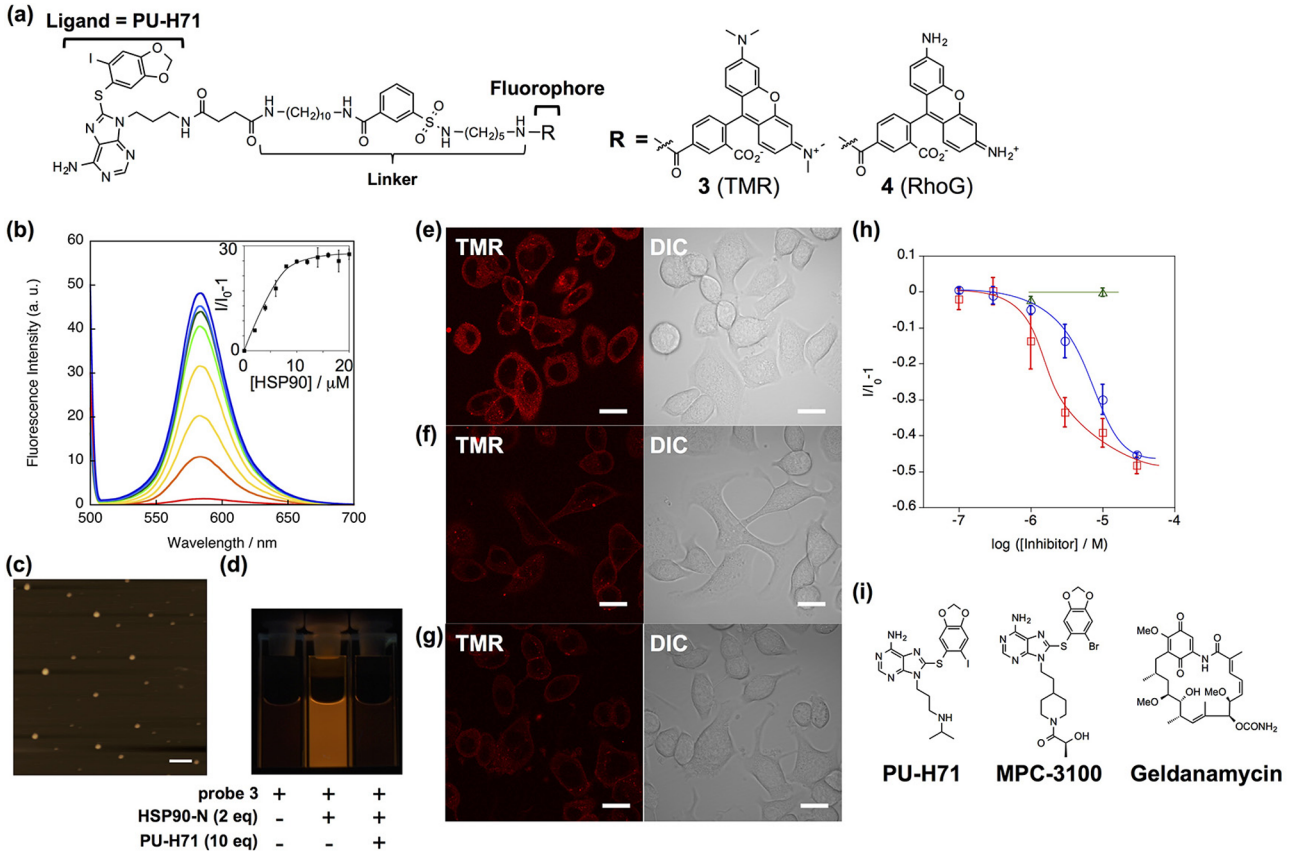

Figure 6. Endogenously expressed intracellular HSP90 imaging and inhibitor assay in living cells by self-assembling nanoaggregates. (a) Chemical structures of ligand-tethered probes **3** and **4** for intracellular endogenous HSP90 imaging. (b) Fluorescence spectra change of probe **3** (10 μM) upon addition of purified HSP90-N (0–20 μM) (λ_{ex} = 480 nm) in 50 mM HEPES buffer. (Inset) Fluorescence titration curve of probe **3** upon addition of HSP90-N (0–20 μM) (λ_{em} = 585 nm). (c) AFM image of probe 3 (10 μM) in 50 mM HEPES buffer. (d) Photographs of probe **3** (10 μM) in the absence or presence of HSP90-N (20 μM, left or middle, respectively), and after addition of PU-H71 (100 μM) to the solution of **3** and HSP90-N (right). (e) CLSM images of SK-BR-3 cells treated with probe **3** (100 nM) for 4 h at 37 °C in cultured media. The images were obtained without any washing (scale bars, 20 μm). (f,g) CLSM images of SK-BR-3 cells treated with probe **3** (100 nM) for 4 h at 37 °C, and then treated with PU-H71 (f, 10 μM) or MPC3100 (g, 30 μM). The images were obtained without any washing (scale bars, 20 μm). (h) Fluorescence titration profile of the relative change in fluorescence intensity ($I/I_0 - 1$) from the intracellular region vs inhibitor concentration for PU-H71 (□, red), MPC-3100 (○, blue) and Geldanamycin (△, green). Fluorescence intensities were evaluated at 10 cells in 5 regions in each dish, and the experiments were performed in triplicate to obtain mean and standard error values (shown as error bars). (i) Chemical structures of HSP90 inhibitors used in this study.

applications in the future. Moreover, it is likely that these reversible self-assembling probes can be adapted for use in fluorescently visualizing a number of intracellular protein functions by varying the ligand and fluorophore.

■ CONCLUSION

In summary, the results indicate that our protein-responsive self-assembling nanoaggregates is applicable for selective and reversible sensing of endogenous proteins even inside living cells. The quantitative study using an overexpressed model protein revealed that the designed probes form self-assembling nanoaggregates in the signal-off mode in living cells in the absence of the target protein, whereas the disassembly driven turn-on fluorescent change is induced in the presence of the target by a specific ligand–protein recognition process. Interestingly, the addition of a competitive inhibitor induced the probe to reassemble so that the fluorescence was turned off, explicitly verifying that the reversible assembly/disassembly of these supramolecular nanomaterials took place even inside the living cells. The intracellular reversibility of the collapse and formation of our self-assembled nanoaggregates is unprecedented. This dynamic sensing mechanism allowed us to construct a quantitative cell-based inhibitor assay for intracellular endogenous proteins such as hCAII and HSP90, two valuable diagnostic and therapeutic protein targets. This work should inspire new research into supramolecular approaches, which work inside cells in a programmable manner for cell-selective tissue engineering,[46] intracellular protein-triggered drug release, or cell signaling modulation.

■ EXPERIMENTAL SECTION

Synthesis. The synthetic procedures used to prepare compounds **1′**, **2**–**4** and characterizations of these compounds are described in the Supporting Information.

General Materials and Methods. Purified human carbonic anhydrase II (hCAII) was purchased from Sigma, and *Escherichia coli* DHFR was prepared and purified as previously reported.[47] Other chemical reagents and solvents were purchased from commercial chemical suppliers (Sigma, Aldrich, TCI, Wako, or Watanabe Chemical Industries) and used without further purification. ^{1}H NMR spectra were recorded on a Varian Mercury-400 spectrometer (400 MHz). High-resolution electrospray ionization Fourier transform mass spectrometry (HR-ESI-MS) spectra were recorded using a

dx.doi.org/10.1021/ja508955y | J. Am. Chem. Soc. 2014, 136, 16635–16642

Thermo Scientific Exactive mass spectrometer. Cell imaging was performed with a confocal laser scanning microscope (CLSM, Olympus, FV1000, IX81) equipped with a 60×, NA = 1.35 oil objective lens. Fluorescence images were acquired using the 488 nm line of an argon laser to excite EGFP (emission, 500−530 nm), the 515 nm line of an argon laser to excite Rho-G (emission, 530−630 nm) and the 543 nm line of a HeNe Green laser to excite tetramethylrhodamine (emission, 555−655 nm). HeLa-DG cells, normal Hela cells, and MCF-7 cells were maintained in DMEM supplemented with 10% fetal bovine serum (FBS), penicillin (100 units/mL), and streptomycin (100 μg/mL) at 37 °C in 5% CO_2 and 95% air. SK-BR-3 cells were maintained in McCoy's 5A Modified Media supplemented with 10% FBS, penicillin (100 units/mL), and streptomycin (100 μg/mL) at 37 °C in 5% CO_2 and 95% air. The cells were plated at a density of 2.0×10^5 cells per a 35 mm glass-bottomed dish and cultured in the medium for 24 h at 37 °C in 5% CO_2 and 95% air and used for fluorescence imaging.

UV−Visible Absorption and Fluorescence Spectroscopic Analyses. All probes were dissolved in dimethyl sulfoxide (DMSO) to generate stock solutions. The concentrations of probes **1′**, **2**, **3**, and **4** were determined by their absorbance (at 543 nm for **1′**, **2** and **3**, 504 nm for **4**) in methanol using a molar extinction coefficient of 92 000 M^{-1} cm^{-1} for **1′**, **2** and **3**, and 78 000 M^{-1} cm^{-1} for **4**,[48] respectively. HCAII was dissolved in PBS buffer (pH 7.2), and HSP90-N was dissolved in 10 mM Tris buffer (pH 7.4). The concentrations of these proteins were determined by their absorbance at 280 nm using literature molar extinction coefficients of 54 000 M^{-1} cm^{-1} for hCAII[49] and 31 100 M^{-1} cm^{-1} for DHFR[50] respectively, and 27 000 M^{-1} cm^{-1} for Hsp90-N, which was determined by its absorption spectra and BCA protein assay kit allowing stock solutions of known concentrations to be prepared. All experiments were performed at 25 °C in test tubes. UV−visible absorption spectra were recorded on a Shimadzu UV−visible 2550 spectrometer. Fluorescence spectra were measured using a PerkinElmer LS55 fluorescent spectrometer. Absorption and fluorescence measurements were performed 30 min after adding the protein to each probe solution (10 μM stock solution).

Fluorescence Imaging of eDHFR with Probe 1. Hela-DG cells and normal Hela cells cultured in DMEM were rinsed with serum- and phenol red-free DMEM supplemented with 100 U/mL penicillin and 100 μg/mL streptomycin ($DMEM_i$, 1 mL), and treated with probe **1** (2 μM, <1% DMSO (v/v)) in $DMEM_i$ (1 mL). Fluorescence imaging was carried out 2, 4, 6, and 12 h after staining without performing any washing. For the control experiments, the cells were treated with probe **1** (2 μM) for 12 h at 37 °C, and then TMP was added (10 μM, <1% DMSO (v/v)), and the fluorescence images were obtained without performing any washing. For examination of the effects of endocytosis inhibitors, cells were treated with probe **1** only (2 μM, <1% DMSO (v/v)), probe **1** (2 μM) and genistein (100 μM), **1** (2 μM) and EIPA (40 μM) or **1** (2 μM) and amantadine (500 μM). After 4 h incubation of these compounds, fluorescence imaging was carried out without performing any washing.

Fluorescence Imaging in MCF7 and SK-BR-3 Cells with Probe 2−4. MCF7 cells plated on a 35 mm glass-bottomed dish were rinsed with $DMEM_i$, and treated with probe **2** (300 nM, <1% DMSO (v/v)) in $DMEM_i$ (1 mL). For the control experiments, after incubation for 4 h, a stock solution of EZA was added (final concentration, 100 μM) to the cells. Fluorescence images were obtained without performing any washing. SK-BR-3 cells plated on the 35 mm glass-bottomed dish were rinsed with $DMEM_i$, and treated with probe **3** or **4** (100 nM, <1% DMSO (v/v)) in $DMEM_i$ (1 mL). After 4 h incubation of these compounds, fluorescence imaging was carried out without performing any washing.

Inhibitor Assay for hCAII in MCF7 Cells. Probe **2** (100 nM) was added to the MCF-7 cells plated on a 35 mm glass-bottomed dish. After incubation for 4 h, a stock solution of each inhibitor was added to the cells. After an additional incubation for 1 h, fluorescence imaging was carried out without performing any washing. To determine the fluorescence intensity in the cell, CLSM images were analyzed with ImageJ 1.44 on a Macintosh PC.

■ ASSOCIATED CONTENT

Ⓢ Supporting Information

Figures, experimental details, and synthetic procedures. This material is available free of charge via the Internet at http://pubs.acs.org.

■ AUTHOR INFORMATION

Corresponding Authors

ytakaoka@m.tohoku.ac.jp
ihamachi@sbchem.kyoto-u.ac.jp

Notes

The authors declare no competing financial interest.

■ ACKNOWLEDGMENTS

We thank Dr. Shinya Tsukiji (Nagaoka University of Technology) for the plasmid encoding pBAD-DHFR and HeLa-DG cells. Prof. K. Matsuda (Kyoto University) and Dr. T. Hirose (Kyoto University) are acknowledged for their assistance with DLS measurements. We thank Prof. K. Akiyoshi (Kyoto University) and Dr. S. Sawada (Kyoto University) for the technical support for flow cytometry. T.Y. and K.M. acknowledge receipt of the JSPS Research Fellowships for Young Scientists. This work was partly supported by a Grant-in-Aid for Young Scientists (A) (No. 25708026), the CK Integrated Medical Bioimaging Project (MEXT) and CREST (Japan Science and Technology Agency).

■ REFERENCES

(1) Giepmans, B. N. G.; Adams, S. R.; Ellisman, M. H.; Tsien, R. Y. *Science* **2006**, *312*, 217−224.

(2) Kobayashi, H.; Ogawa, M.; Alford, R.; Choyke, P. L.; Urano, Y. *Chem. Rev.* **2010**, *110*, 2620−2640.

(3) Zhang, H.; Fan, J.; Wang, J.; Zhang, S.; Dou, B.; Peng, X. *J. Am. Chem. Soc.* **2013**, *135*, 11663−11669.

(4) Tang, R.; Kim, C. S.; Solfiell, D. J.; Rana, S.; Mout, R.; Velázquez-Delgado, E. M.; Chompoosor, A.; Jeong, Y.; Yan, B.; Zhu, Z.-J.; Kim, C.; Hardy, J. A.; Rotello, V. M. *ACS Nano* **2013**, *7*, 6667−6673.

(5) (a) Azagarsamy, M. A.; Yesilyurt, V.; Thayumanavan, S. *J. Am. Chem. Soc.* **2010**, *132*, 4550−4551. (b) Guo, J.; Zhuang, J.; Wang, F.; Raghupathi, K. R.; Thayumanavan, S. *J. Am. Chem. Soc.* **2014**, *136*, 2220−2223.

(6) You, C.-C.; Miranda, O. R.; Gider, B.; Ghosh, P. S.; Kim, I.-B.; Erdogan, B.; Krovi, S. A.; Bunz, U. H. F.; Rotello, V. M. *Nat. Nanotechnol.* **2007**, *2*, 318−323.

(7) Cabral, H.; Nishiyama, N.; Kataoka, K. *Acc. Chem. Res.* **2011**, *44*, 999−1008.

(8) Sapsford, K. E.; Algar, W. R.; Berti, L.; Gemmill, K. B.; Casey, B. J.; Oh, E.; Stewart, M. H.; Medintz, I. L. *Chem. Rev.* **2013**, *113*, 1904−2074.

(9) Liang, G.; Ren, H. J.; Rao, J. H. *Nat. Chem.* **2010**, *2*, 54−60.

(10) Ye, D.; Shuhendler, A. J.; Cui, L.; Tong, L.; Tee, S. S.; Tikhomirov, G.; Felsher, D. W.; Rao, J. *Nat. Chem.* **2014**, *6*, 519−526.

(11) Gao, Y.; Shi, J. F.; Yuan, D.; Xu, B. *Nat. Commun.* **2012**, DOI: 10.1038/ncomms2040.

(12) Li, J.; Gao, Y.; Kuang, Y.; Shi, J.; Du, X.; Zhou, J.; Wang, H.; Yang, Z.; Xu, B. *J. Am. Chem. Soc.* **2013**, *135*, 9907−9914.

(13) Ding, D.; Kai, L. K.; Liu, B.; Tang, B. Z. *Acc. Chem. Res.* **2013**, *46*, 244−2453.

(14) Shi, H.; Liu, J.; Geng, J.; Tang, B. Z.; Liu, B. *J. Am. Chem. Soc.* **2012**, *134*, 9569−9572.

(15) Shi, H.; Kwok, R. T. K.; Liu, J.; Xing, B.; Tang, B. Z.; Liu, B. *J. Am. Chem. Soc.* **2012**, *134*, 17972−17981.

(16) Takaoka, Y.; Sakamoto, T.; Tsukiji, S.; Narazaki, M.; Matsuda, T.; Tochio, H.; Shirakawa, M.; Hamachi, I. *Nat. Chem.* **2009**, *1*, 557−561.

(17) Takaoka, Y.; Kiminami, K.; Mizusawa, K.; Matsuo, K.; Narazaki, M.; Matsuda, T.; Hamachi, I. *J. Am. Chem. Soc.* **2011**, *133*, 11725−11731.
(18) Mizusawa, K.; Ishida, Y.; Takaoka, Y.; Miyagawa, M.; Tsukiji, S.; Hamachi, I. *J. Am. Chem. Soc.* **2010**, *132*, 7291−7293.
(19) Mizusawa, K.; Takaoka, Y.; Hamachi, I. *J. Am. Chem. Soc.* **2012**, *134*, 13386−13995.
(20) Ishida, M.; Watanabe, H.; Takigawa, K.; Kurishita, Y.; Oki, C.; Nakamura, A.; Hamachi, I.; Tsukiji, S. *J. Am. Chem. Soc.* **2013**, *135*, 12684−12689.
(21) Baccanari, D. P.; Daluge, S.; King, R. W. *Biochemistry* **1982**, *21*, 5068−5075.
(22) Miller, L. W.; Cai, Y.; Sheetz, M. P.; Cornish, V. W. *Nat. Methods* **2005**, *2*, 255−257.
(23) From the intra- and extracellular fluorescent intensity in CLSM images in Figure S3e, the intracellular concentration of probe **1**′ was roughly estimated.
(24) Parton, R. G.; Joggerst, B.; Simons, K. *J. Cell Biol.* **1994**, *127*, 1199−1215.
(25) Swanson, J. A.; Watts, C. *Trends Cell Biol.* **1995**, *5*, 424−428.
(26) Meier, O.; Boucke, K.; Hammer, S. V.; Keller, S.; Stidwill, R. P.; Hemmi, S.; Greber, U. F. *J. Cell Biol.* **2002**, *158*, 1119−1131.
(27) Phonphok, Y.; Rosenthal, K. S. *FEBS Lett.* **1991**, *281*, 188−190.
(28) Petros, R. A.; DeSimone, J. M. *Nat. Rev. Drug Discovery* **2010**, *9*, 615−627.
(29) Nakata, E.; Yukimachi, Y.; Nazumi, Y.; Uwate, M.; Maseda, H.; Uto, Y.; Hashimoto, T.; Okamoto, Y.; Hori, H.; Morii, T. *RSC Adv.* **2014**, *4*, 348−357.
(30) Supuran, C. T. *Nat. Rev. Drug Discovery* **2008**, *7*, 168−181.
(31) The quantitative comparison between the intra- and extracellular fluorescent intensity in CLSM images revealed that the probe **2** (extracellular concentration was 100 nM) was concentrated into the cell inside by 6.7-fold even in the presence of EZA (1 μM), which enabled us to roughly estimate the intracellular concentration of probe **2** to be at least 670 ± 220 nM (Figure S5e). This value was higher than the CAC of **2** (110 nM) determined by the test tube experiments. Thus, it is conceivably indicated that the nanoprobe **2** could be self-assembled in the cell interior.
(32) Under these conditions, almost no cytotoxicity was observed (Figure S5g).
(33) Casini, A.; Abbate, F.; Scozzafava, A.; Supuran, C. T. *Bioorg. Med. Chem. Lett.* **2003**, *13*, 2759−2763.
(34) Trepel, J.; Mollapour, M.; Giaccone, G.; Neckers, L. *Nat. Rev. Cancer* **2010**, *10*, 537−549.
(35) Chiosis, G.; Neckers, L. *ACS Chem. Biol.* **2006**, *1*, 279.
(36) He, H.; Zatorska, D.; Kim, J.; Aguirre, J.; Llauger, L.; She, Y.; Wu, N.; Immormino, R. M.; Grewirth, D. T.; Chiosis, G. *J. Med. Chem.* **2006**, *49*, 381−390.
(37) Modi, S.; Stopeck, A.; Linden, H.; Solit, D.; Chandarlaaty, S.; Rosen, N.; D'Andrea, G.; Dickler, M.; Moynahan, M. E.; Sugarman, S.; Ma, W.; Patil, S.; Norton, L.; Hannah, A. L.; Hudis, C. *Clin. Cancer Res.* **2011**, *17*, 5132−5139.
(38) Prodromou, C.; Piper, P. W.; Peal, L. H. *Proteins* **1996**, *25*, 517−522.
(39) Maroney, A. C.; Marugan, J. J.; Mezzasalma, T. M.; Barnakov, A. N.; Garrabrant, T. A.; Weaner, L. E.; Jones, W. J.; Barnakova, L. A.; Koblish, H. K.; Todd, M. J.; Mascussi, J. A.; Deckman, I. C.; Galemmo, R. A., Jr.; Johnson, D. L. *Biochemistry* **2006**, *45*, 5678−5685.
(40) Chiosis, G.; Timaul, M. N.; Munster, P. N.; Zheng, F. F.; Sepp-Lorenzino, L.; Rosen, N. *Chem. Biol.* **2011**, *8*, 289−299.
(41) Taldone, T.; Gomes-DaGama, E. M.; Zong, H.; Sen, Siddhartha; Alpaugh, M. L.; Zatorska, D.; Alonso-Sabadell, R.; Guzman, M. L.; Chiosis, G. *Bioorg. Med. Chem. Lett.* **2011**, *21*, 5347−5352.
(42) Similar to probe **2**, the intra- and extracellular fluorescent intensity in CLSM images showed that the intracellular concentration of probe **3** (extracellular concentration was 100 nM) was roughly estimated to be at least 1.1 ± 0.3 μM even in the presence of PU-H71 (10 μM) (Figure S11b). This value was higher than the CAC of **3** (110 nM) determined by the test tube experiments. Thus, it is conceivable indicated that the nanoprobe **3** could be self-assembled in the cells interior.
(43) Similar to probes **1** and **2**, almost no cytotoxity was observed both in cases of probes **3** and **4** (Figure S12d and S14d).
(44) Kim, S.-H.; Bajji, A.; Tangallapally, R.; Markovitz, B.; Trovato, R.; Shenderovich, M.; Baichwal, V.; Bartel, P.; Cimbora, D.; McKinnon, R.; Robinson, R.; Panac, D.; Wettstein, D.; Carlson, R.; Yager, K. M. *J. Med. Chem.* **2012**, *55*, 7480−7501.
(45) Hartmann, F.; Horak, E. M.; Cho, C.; Lupu, R.; Bolen, J. B.; Steler-Stevenson, M. A.; Pfreundschuh, M.; Waldmann, T. A.; Horak, I. D. *Int. J. Cancer* **1997**, *70*, 221−229.
(46) Hirata, N.; Nakagawa, M.; Fujibayashi, Y.; Yamauchi, K.; Murata, A.; Minami, I.; Tomioka, M.; Kondo, T.; Kuo, T.-F.; Endo, H.; Inoue, H.; Sato, S.; Ando, S.; Kawazoe, Y.; Aiba, K.; Nagata, K.; Kawase, E.; Chang, Y.-T.; Suemori, H.; Eto, K.; Nakauchi, H.; Yamanaka, S.; Nakatsuji, N.; Ueda, K.; Uesugi, M. *Cell Rep.* **2014**, *6*, 1165−1174.
(47) Tanaka, T.; Kamiya, N.; Nagamune, T. *FEBS Lett.* **2005**, *579*, 2092−2096.
(48) Haugland, R. P. *The Handbook: A Guide to Fluorescent Probes and Labeling Technologies*, 10th ed.; Invitrogen: Carlsbad, CA, 2005.
(49) Supuran, C. T.; Briganti, F.; Tilli, S.; Chegwidden, W. R.; Scozzafava, A. *Bioorg. Med. Chem.* **2001**, *9*, 703−714.
(50) Touchette, N. A.; Perry, K. M.; Matthews, C. R. *Biochemistry* **1986**, *25*, 5445−5452.